Passive Radar detection of small UAV over sea

Idar Norheim-Næss, Erlend Finden, Kyrre Strøm

Norwegian Defence Research Establishment (FFI)
P.O. Box 25, NO-2027 Kjeller, Norway
email: idar.norheim-nass@ffi.no, erlend.finden@ffi.no, kyrre.strom@ffi.no

Abstract: *During a trial over the Trondheim-fjord in Norway fall 2018, a DVB-T based passive radar system was used for detecting a small unmanned aerial vehicle (UAV) over sea. The measurements show a possible detection range of 1 km radial range away from the radar receiver and with terrain masking of the direct signal interference from the transmitter to the receiver. Strong multipath from the sea match well with simulations. The multipath will, with a single receiver channel, severely affect the radar performance, but this could for shorter detection distances be mitigated by using two to three receiver channels at differing altitude, with the benefit of an additional gain of up to 6dB caused by the multipath.*

1. Introduction

Passive radar is well described in [1]. An issue in passive radar is that the strong reference signal from the transmitter and other interference may mask the weaker target echo in the receiver surveillance channel. A method of reducing this is to generate nulls in the radiation pattern of the antenna in the direction of the reference signal [2]. Some studies have claimed to increase detection range by reducing the interference by applying a cross-polarized surveillance antenna with respect to the transmitter, arguing that the cross-polarized radar cross section (RCS) is sufficient to give a net increase in signal-to-Noise-Ratio (SNR) [3][4][5]. Studies done at FFI suggests that the decrease in direct signal interference does not always weigh out the decrease in cross-polarized RCS [6], and increasing the detection range of the passive radars against small targets is wanted. The old idea of terrain masking for direct signal suppression is therefore still highly relevant.

In the fall of 2018, a measurement campaign was held over the Trondheim-fjord in Norway, where a small unmanned aerial vehicle (UAV) of type DJI Mavic Pro was used as test target against a DVB-T based passive radar. The scope of the campaign was to evaluate the possible detection performance against small targets in the area. Measurements were performed at the location, and then combined with electromagnetic simulations of the radar cross section (RCS) of a computer aided design (CAD) model of the drone, in order to predict the sensor coverage also for other targets. Terrain masking for suppressing the direct signal from the transmitter to the radar, in combination with a directive antenna pointing away from mountainous areas reflecting the direct signal was used to increase the detection sensitivity of the system.

DOI til publisert versjon/DOI to published version: 10.23919/IRS.2019.8768179

2. Measurement setup

The measurement was done in Viken at Inderøy island in the Trondheim-fjord area. The area was selected for a combination of strong TV signal from the Mosvik transmitter (49kW EIRP, 23.7 km away), and terrain screening of the same signal between the transmitter and the surveillance antenna. The system was placed with a 150m cable from the receiver to a reference antenna at elevated grounds, using a band pass filter and 30W Mini Circuits ZHL-30W-252+ amplifier to transport the signal to the receiver. The surveillance antenna was placed approximately 12m from the radar receiver, pointing North and away from the transmitter. The setup is shown in Figure 1.

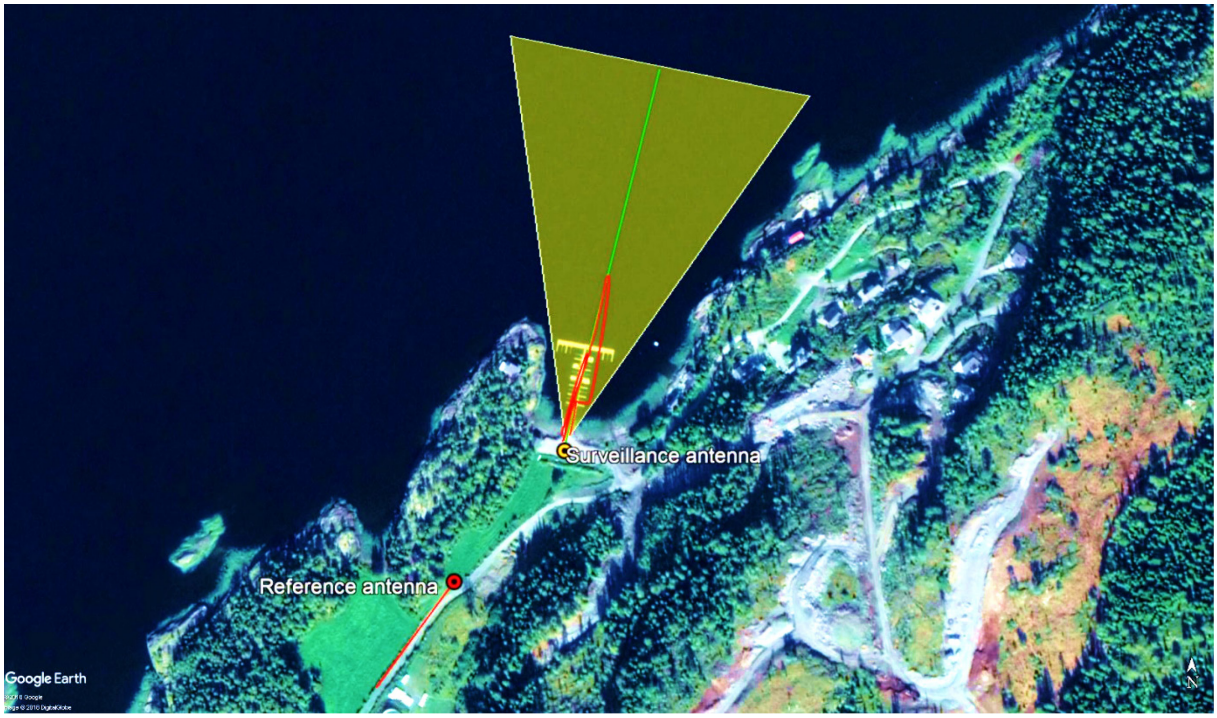

Figure 1. Measurement setup at Viken, Inderøy, Norway. Reference antenna was pointing in direction of the red line, surveillance antenna was pointing along the green line, and an example UAV flight is shown as a red track within the yellow area indicating an approximate antenna coverage.

The Atlantis DVB-T based passive radar, developed by Fraunhofer FHR in Germany, is a 12-channel sensor capable of real-time digital beamforming and recording of 12 32-MHz channels. During this trial, two channels were used for processing a single reference and single surveillance channel. The system uses a double conversion super-heterodyne design, based on very low phase noise synthesizers for down conversion and digitization. The digitizers are designed by Fraunhofer FHR, and a detailed description of the system can be found in [7].

The reference receiver antenna was a simple Yagi-Uda design, and the surveillance antenna was a “Televes DAT HD 75 BOSS” with 19dB gain and 27° horizontal beam width shown in Figure 2.

Dette er en postprint-versjon/This is a postprint version.
DOI til publisert versjon/DOI to published version: 10.23919/IRS.2019.8768179

Figure 2. Televes DAT HD 75 BOSS antenna for surveillance.

Figure 3. DJI Mavic Pro. Picture from [8].

The UAV used was of type DJI Mavic Pro, shown in Figure 3. The UAV was flown with a minimum of attitude changes to simplify the RCS simulations. A single direction defined by the direction of a pier was chosen, and the drone flown radially in this direction with constant velocity. Two different velocities were used, and the direction of the UAV flown in two directions to show the front and rear. The altitude of the UAV was 19m over the WGS84 geoid.

3. Target RCS simulations

The DJI Mavic UAV is comparable to the wavelength used. The broadcast signal of 682MHz has a wavelength of 44cm, and the drone has a maximum size of 33.5 cm diagonally (excluding propellers). The propellers are made of plastic and expected to contribute insignificantly to the RCS. The drone internals were examined, and the main contributing parts consisting of the motors, cabling, antennas and electronics were located. The front part with the camera is excluded, and the model is expected to give less accurate simulation results in this direction. The CAD-model is shown in Figure 4.

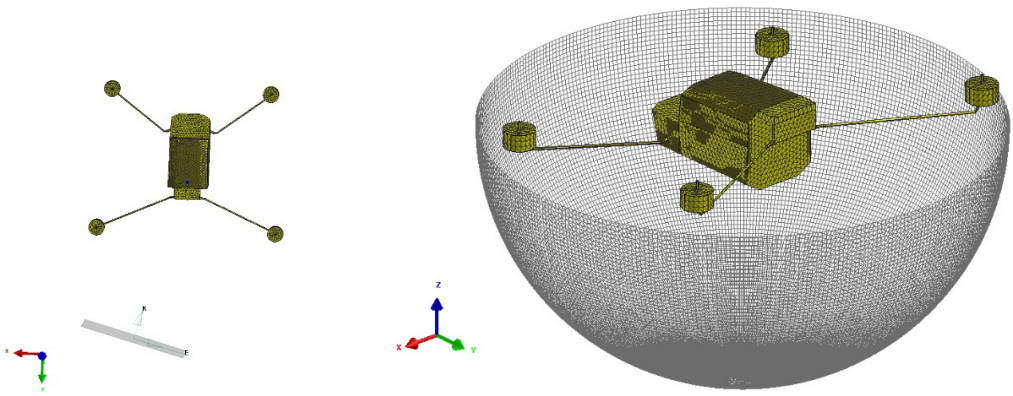

Figure 4. DJI Mavic Pro simplified CAD model for RCS simulations.

With the transmitter at almost 30km distance, the UAV flying radially in relation to the radar and close to radially away from the transmitter, and the UAV keeping relatively constant attitude towards the receiver, the bistatic calculations could be simplified. The geometry was further simplified by only using data outside 80 meter radial range, to make sure the UAV was within the main lobe of the receiver antenna and the scattering angle varying little.

Dette er en postprint-versjon/This is a postprint version.
DOI til publisert versjon/DOI to published version: 10.23919/IRS.2019.8768179

Simulations on this CAD-model was then performed in software by ESI Group, corresponding to the horizontally and co-polarised (HH) measurement setup. In Figure 5 the RCS simulation results can be seen where the blue line is the UAV flying with its front towards the radar, and the red flying with the rear towards the radar. The angles along the horizontal axis represent different forward tilt angles of the UAV. During the flight a forward tilt of approximately 7 degrees were observed, giving a scattering angle (Theta_s, vertical angle from zenith) of 97 degrees. For the scattering angles relevant to the detection data being analyzed (90°-110°) the RCS is around -22.5dBsm (0.006 m^2) for the rear of the UAV and -20dBsm (0,01m^2) for the front.

Considering the diagonal size of the UAV relative to the wavelength, it should in the monostatic case be in the resonant region. The simulations seem to indicate that the bistatic RCS is small, and that the UAV should be challenging to detect at larger distances. More analysis should be done, and the sensitivity to more bistatic geometries assessed, for evaluating the uncertainty in recalculating the detection ranges for other target types.

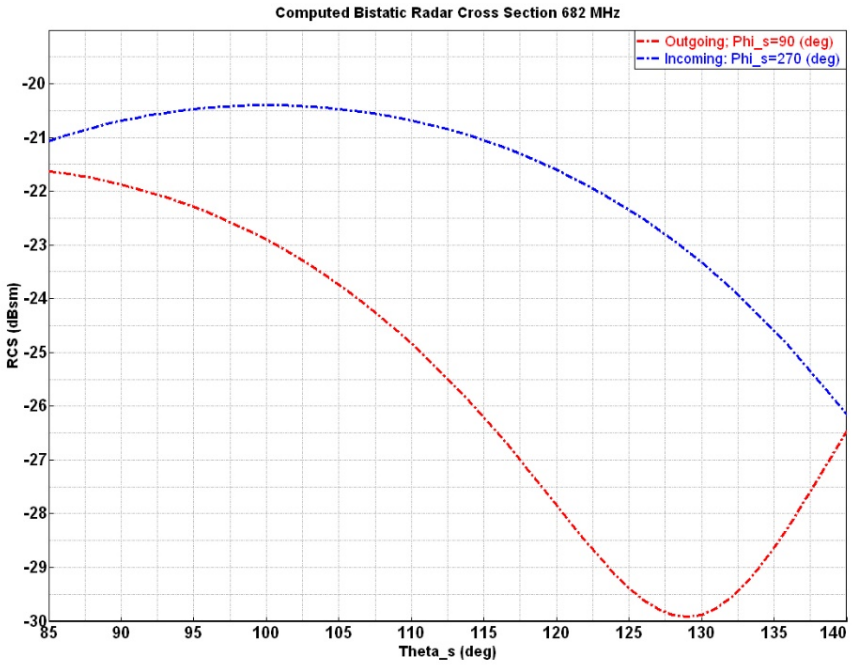

Figure 5. RCS simulations for a simplified DJI Mavic Pro. The angle along the horizontal axis shows the RCS' sensitivity to the tilt angle of the UAV. For the data analyzed, Theta_s angles within 90-110 degrees were used.

4. Results

Figure 6 is showing a time interval of the UAV flight, where the horizontal axis on the plot is Doppler and the vertical bistatic range in km. The line at 0 Hz Doppler represents the ground clutter received by the surveillance antenna. The UAV started at 0 range and -12Hz Doppler, continuing out to 600 meter bistatic range, turned and flew at +40 Hz Doppler radially todwards the radar again. Figure 7 and Figure 8 shows the detections used for the data analysis, from an other time interval. Detections were extracted by calculating the noise floor in a corner of the range-Doppler map without targets present, and using cells above 18dB Signal-to-Interference-and-Noise (SINR) and above ±10Hz to exclude sea-clutter and ground clutter. Figure 7 shows only detections that is less than 100 m and 40 Hz away from the corresponding bistatic range and Doppler of the drone obtained from the GPS position to the drone.

Dette er en postprint-versjon/This is a postprint version.
DOI til publisert versjon/DOI to published version: 10.23919/IRS.2019.8768179

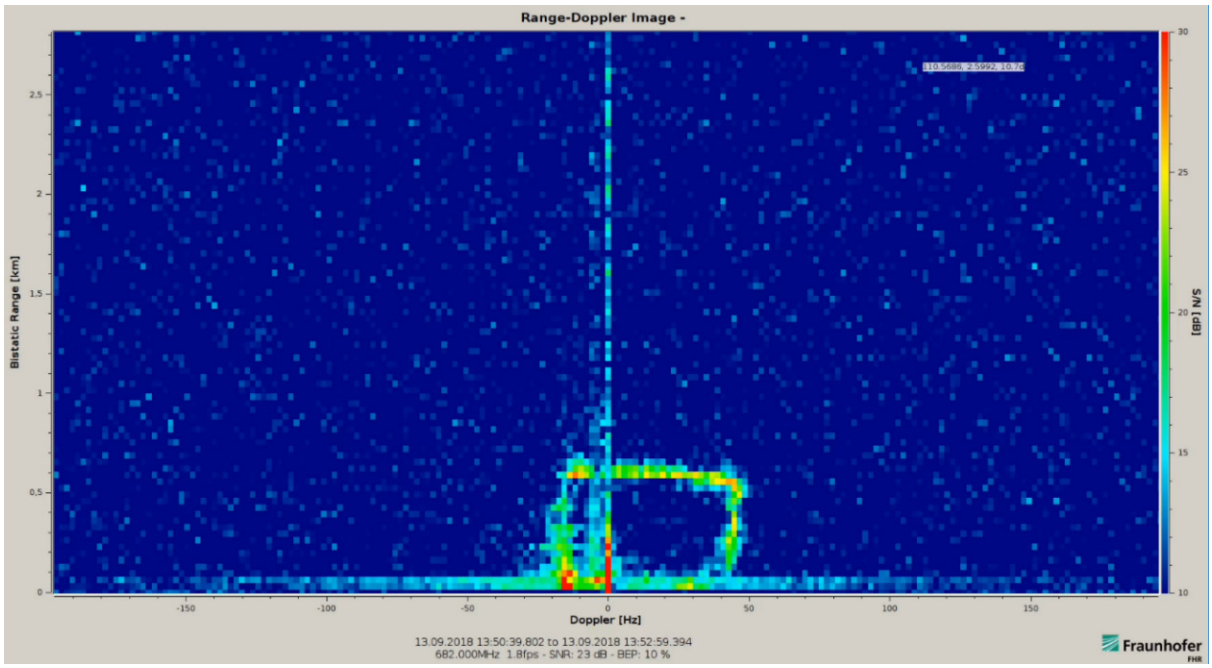

Figure 6. UAV has been visible out to approximately 600m bistatic range, with Doppler at +18Hz at cruise speed outbounds, and more than -40 Hz full speed inbounds. The horizontal axis is Doppler in Hz, and the vertical axis is bistatic range.

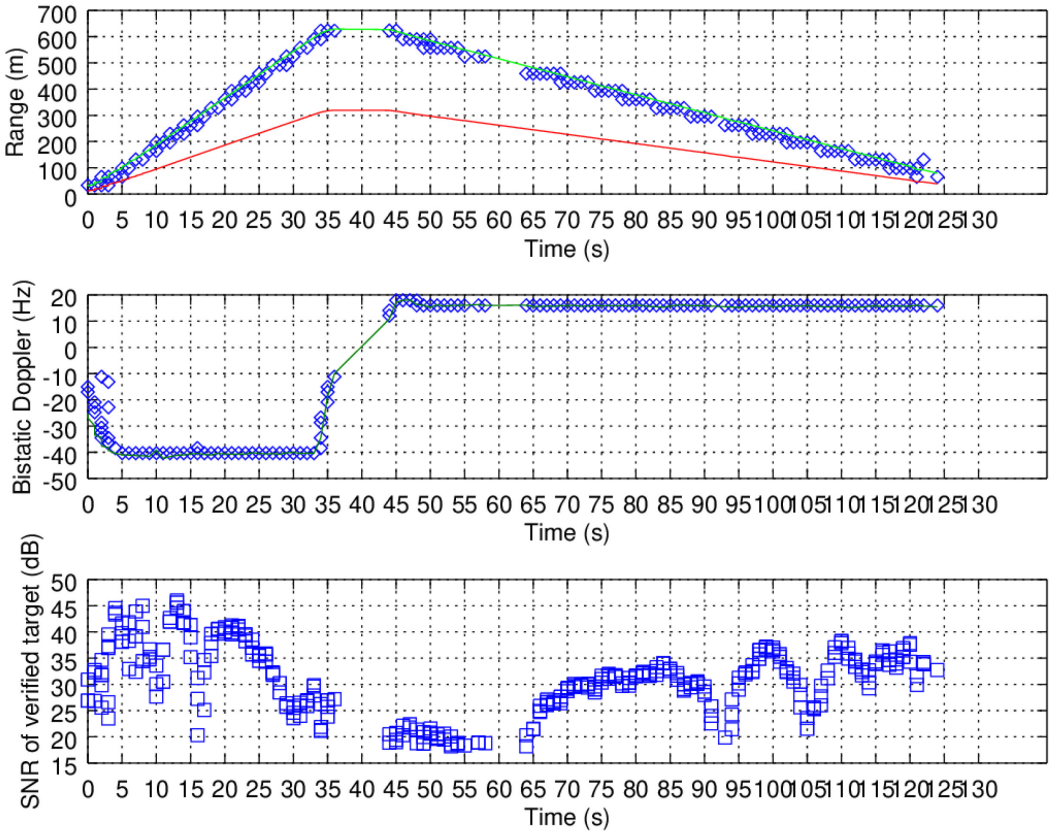

Figure 7. Upper panel: GPS-position of the UAV in bistatic range as the green line. Detections above 18dB SINR and associated with target GPS is shown as blue squares. The red line shows radial range from radar to the drone.
Mid panel: GPS-position of drone in bistatic Doppler as the green line.
Lower panel: Signal-to-interference ratio of the detections associated with the UAV GPS.

Dette er en postprint-versjon/This is a postprint version.
DOI til publisert versjon/DOI to published version: 10.23919/IRS.2019.8768179

In Figure 8 the UAV is cleraly visible at 600 meter bistatic range, corresponding to appr. 320 meter radial range. The multipath effects are highly visible in the upper panel, and the theoretically calculated multipath shown in the middle panel is corresponding well with the nulling areas of the measured results except at 190m. The multipath calculations assume perfect reflection and an electromagnetic smooth surface. The multipath propagation from transmitter to target is varying little because of the larger distance, but may become significant for targets at other ranges.

In Figure 8, the outbound target has an SINR 5-8 dB higher than the inbound. The simulations in Figure 5 show a smaller RCS for the rear of the drone, indicating that there indeed are some uncertanities in the simulations. This may stem from the simplified model not being detailed enough.

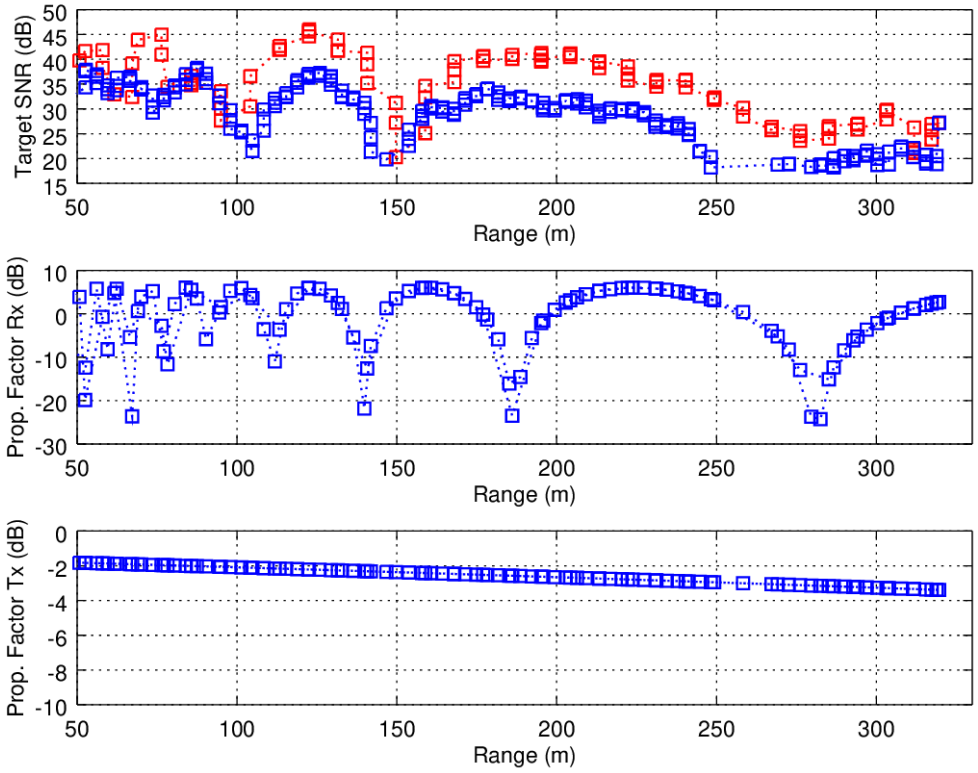

Figure 8. Upper panel show target detections SINR for radial range to radar, where the stronger red SINR values represent the outbound UAV. The middle panel show the calculated multipath propagation factor from target to receiver, and the lower panel show calculated multipath propagation factor for transmitter to target.

Krysztof Kulpa et. al. have in [9] written an article on the theoretical calculations of multipath effects in passive radar systems. A simple sketch of multipath and its implications is shown in Figure 9. A specular reflection from ground/sea will create a signal with a delayed phase, and if the delay is within a range resolution cell of the system the received signal may cancel out if out of phase. This will create areas where targets will be undetectable for a radar receiver with an antenna at a single height. For the calculations here, where the distance from target to receiver is very short, only flat-earth geometries are used. In addition, the target is known to be flying at an altitude lower than the range-cell widths of the signal, so that multiple detections from the test target and its multipath will not occur. We may therefore assume the target energy and multipath energy to coherently sum for the whole duration of the experiment.

Dette er en postprint-versjon/This is a postprint version.
DOI til publisert versjon/DOI to published version: 10.23919/IRS.2019.8768179

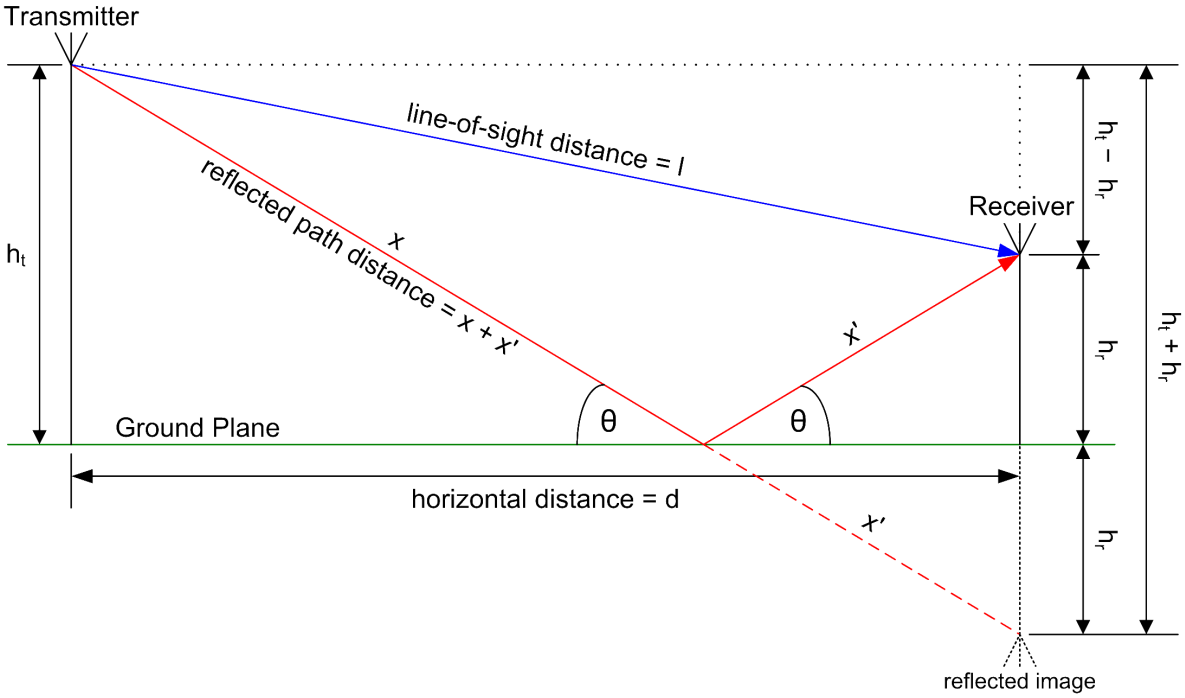

Figure 9. Illustration of multipath geometry, where the direct signal (blue) and specular reflected signal (red) are summed at the receiver. Illustration made by Derek Chandler (Wikimedia Commons).

Theoretical calculations of one-way multipath versus distance is plotted in Figure 10 for three different antenna heights. From these calculations it is evident that the multipath is highly dependent on the antenna height, and therefore also on tide elevations. In the area of the measurements, tides of more than 3.5 meters can be observed. The areas of multipath cancellation can be predicted using tables of tide. Studying the nulling-distances in Figure 10, one may observe that for the ranges calculated for here, using two to three receiver channels at different altitude could mitigate much of the multipath and avoid the long stretches of cancellation and track breaks that would otherwise occure. For longer detection distances one can see in Figure 10 that the nulls may coincide, and the necessary elevation separation between the elements to mitigate the nulls may become unfeasible. Using the technique described by Janusz Kulpa et.al. in [10], or by comparing the received target strenght between the differing channels, the altitude of the target could also potentially be estimated (taking into account the tidal height).

Dette er en postprint-versjon/This is a postprint version.
DOI til publisert versjon/DOI to published version: 10.23919/IRS.2019.8768179

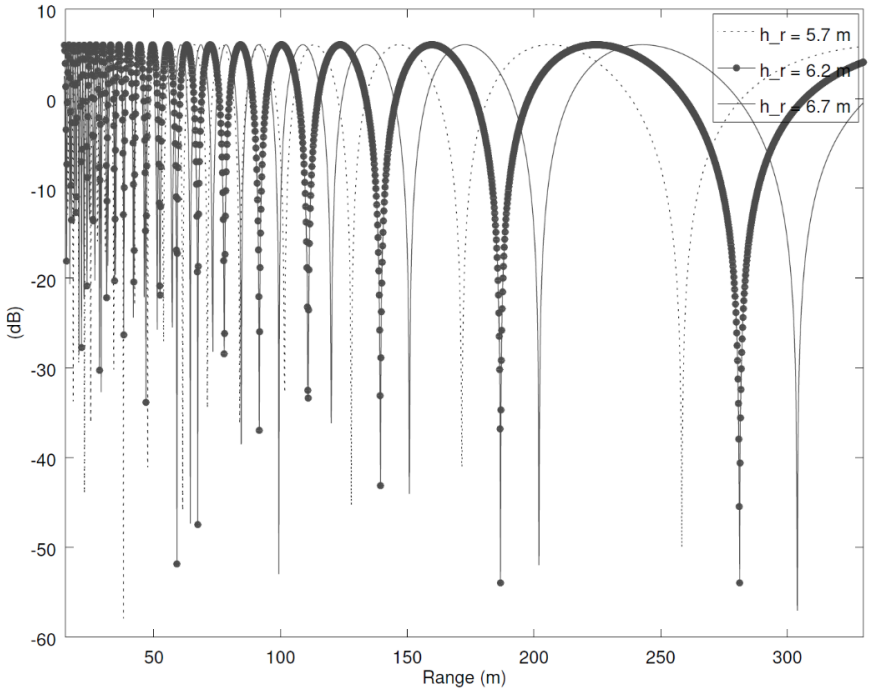

Figure 10. Calculated one-way multipath propagation factor from target to receiver. Two receiver antennas with as little as 1m elevation difference may for closer ranges mitigate much of the nulling problems affecting detection performance over sea.

From M. Cherniakov's book on Bistatic Radar [11] the bistatic radar equation from page 251 looks like:

$$\frac{P_r}{P_n} = \frac{P_t G_t}{4\pi {r_1}^2} \sigma_b \frac{1}{4\pi {r_2}^2} \frac{G_r \lambda^2}{4\pi} \frac{1}{kT_0 BF} L \tag{1}$$

where
P_r = received signal power
P_n = received noise power
P_t = transmit power
G_t = transmit antenna gain
r_1 = transmitter to target range
σ_b = target bistatic radar cross-section
r_2 = target to receiver range
G_r = receive antenna gain
λ = signal wavelength
k = Bolzmann's constant
T_0 = noise reference temperature, 290K
B = receiver effective bandwidth
F = receiver effective noise figure
L = system losses

We may set P_t, G_t, G_r, λ, k, T_0, B, F, and L constant. Because of the relatively small changes of r_1, this variable may for short distances also be included in the constant, reducing the equation to:

$$\frac{P_r}{P_n} = K_1 \frac{\sigma_b}{{r_2}^2} \tag{2}$$

DOI til publisert versjon/DOI to published version: 10.23919/IRS.2019.8768179

Using the RCS of 0.006m^2 of the UAV, and recognizing that the peaks in detection SINR (visible in Figure 8) represents a 6dB coherent addition to the signal caused by the multipath that should be subtracted, we may by using the detections at 125m range, Pr/Pn = 37dB-6dB, calculate the constant K_1 for the UAV to be 95.2dB. Maximum detection range for the UAV given a minimum detection SINR of 12dB will be approximately 1.1 km, on the radial along the extended baseline between transmitter and receiver. If we calculate for an optimistic range by using the stronger reflections of the outbound flight, the estimated detection range can be upwards to 2.8 km

If, by using the sea surface multipath to ones benefit, the 6 dB multipath gain may result in a doubling of the range of the UAV detection.

Expecting longer distances for a standard target of 1m^2, the equation will need to account for the changing distance of transmitter to target as well (see equation 3).

$$\frac{P_r}{P_n} = K_2 \frac{\sigma_b}{(D+r_2)^2 r_2{}^2} \tag{3}$$

Calculating for detections on the extended baseline where $r_1 = D + r_2$ (where D is the baseline between transmitter and receiver), and solving the fourth order equation for r_2 using the more pessimistic detections of the measured data, a detection range of approximately 10.5 km (radial range) can be expected, not accounting for other transmission losses. One may expect the multipath cancellation to be dominating at larger distances over sea, possibly reducing this detection range significantly for low-flying targets.

5. Conclusions

With optimizations including high power transmitter, terrain masking, and directional surveillance antenna, a radial detection range of more than 1.1 km against a small UAV has been estimated based on measurement data for shorter ranges. Powerful multipath can be expected over sea, cancelling out the signal at predictable ranges. If using multiple surveillance antennas at differing altitudes, the nulling may be mitigated at least for shorter detection distances.

Extrapolating the detection distance for a 1m^2 target, based on electromagnetic RCS simulations of a model of the UAV, suggests detection ranges over 10km radially along the extended baseline and away from the transmitter for larger targets.

Usage of UAVs for sensor performance assessment is feasible, but a better verification of the simplified CAD-model should be done. One cannot expect a very high degree of certainty, for which a more deterministic target should be used. A UAV RCS around and slightly below 0.01m^2 is observed in the simulations.

6. Acknowledgements

FFI would like to thank the passive radar group at Fraunhofer FHR for their cooperative spirit, drive in the respective scientific field, and help in running the passive radar!

DOI til publisert versjon/DOI to published version: 10.23919/IRS.2019.8768179

References

[1] P. E. Howland, H. D. Griffiths and C. J. Baker, Passive Bistatic Radar Systems: Emerging Technology, M. Cherniakov, Ed., West Sussex: Wiley, 2008, pp. 247-313.

[2] H. D. Griffiths and N. R. W. Long, "Television-based bistatic radar," in IEE Proceedings F - Communications, Radar and Signal Processing, Dec. 1986.

[3] R. Saini, M. Cherniakov and V. Lenive, "Direct path interference suppression in bistatic system: DTV based radar," Radar Conference 2003, Proceedings of the International IEEE, pp. 309-314, 2003.

[4] C. Coleman and H. Yardley, "Passive bistatic radar based on target illuminations by Digital Audio Broadcasting," Radar, Sonar & Navigation, IET, vol. 2, no. 5, pp. 366-375, 2008.

[5] C. Coleman, R. Watson and H. Yardley, "A practical bistatic passive radar system for use with DAB and DRM illuminators," in Proc. 2008 IEEE Radar Conference, Rome, 2008.

[6] Kyrre Strøm, Øystein Lie-Svendsen, Erlend Finden, Idar Norheim-Næss, Terje Johnsen, Aurora Baruzzi, "DVB-T passive radar dual polarization measurements in the presence of strong direct signal interference", 2017 18th International Radar Symposium (IRS), 2017, Prague, Czech Republic.

[7] J. Schell, J. Heckenbach and H. Kuschel, "ATLANTIS, a scalable, modular PCL receiver for OFDM signals," in *NATO SET-187 Specialist Meeting on Passive Radar, challenges concerning theory and practice in military application*, Szczecin, Poland, 13-14.05.2013.

[8] DJI, "DJI Mavic Pro webpage", *https://www.dji.com/no/mavic*, Visited Jan. 03 2019,

[9] Krzysztof Kulpa, Mateusz Malanowski, Piotr Samczynski, Multipath illumination effects in passive radars, 2011 12th International Radar Symposium (IRS), 2011, Leipzig, Germany

[10] J. Kulpa, Jacek Misiurewicz, "Compressed sensing application for target elevation estimation via multipath effect in a passive radar", 2013 14th International Radar Symposium (IRS), 19-21 June 2013, Dresden, Germany.

[11] Mikhail Cherniakov, "Bistatic Radar emerging technology", 2008, John Wiley & Sons Ltd, West Sussex, England

DOI til publisert versjon/DOI to published version: 10.23919/IRS.2019.8768179